Control and Cybernetics
vol. **55** (2026) No. 1
pages: 65-100
DOI: 10.2478/candc-2026-0004

Transitions between disease-free and endemic states in a controlled epidemic system with non-monotonic incidence framework*

by

G. Swathi[1], G. S. Mahapatra[1*], Prasun Santra[2] and R. Prem Kumar[3]

[1]Department of Mathematics, National Institute of Technology Puducherry, Karaikal-609609, India
[2]Maulana Abul Kalam Azad University of Technology, Kolkata–700064, India
[3]Department of Mathematics, Avvaiyar Government College for Women, Karaikal-609602, Puducherry, India, Affiliated to Pondicherry University, Puducherry- 605014, India
swathigt.maths@gmail.com, gs.mahapatra@nitpy.ac.in*, prasunsantra5@gmail.com, premmaths.agcw@gmail.com
*corresponding author

Abstract: Epidemic outbreaks continue to pose serious global health challenges, demanding, in particular, efficient mathematical tools for understanding and controlling disease transmission. This study employs a non-monotonic incidence rate combined with optimal control theory to capture realistic behavioral responses during epidemics. The work integrates parameter estimation, sensitivity analysis, and bifurcation analysis to identify the key factors affecting disease spread and stability transitions. The basic reproduction number is derived, and its sensitivity to key parameters is quantified. Using Pontryagin's Maximum Principle, optimal strategies are developed to minimize infections and control costs. The model is calibrated with real-world data from selected countries, confirming its relevance to actual epidemics. The analysis reveals that a forward bifurcation governs the transition between disease-free and endemic equilibria, providing crucial insight into stability changes as parameters vary. Overall, the results indicate how optimized control strategies can reduce infection burdens, offering valuable guidance for public health policy and long-term epidemic management.

Keywords: epidemic model; stability of equilibrium; forward sensitivity index; parameter estimation; forward bifurcation; optimal control

*Submitted: September 2025; Accepted: January 2026.

1. Introduction

Understanding the dynamic behaviors and developing effective control strategies for ecological and epidemiological models constitute an essential foundation for advancing the study and management of complex biological systems. The global community continues to witness the ongoing spread of numerous coronavirus variants. WHO helped coordinate global responses, provide evidence-based guidelines, and assist countries with mitigation and vaccination strategies, see World Health Organization (2024), Kordt et al. (2025). While individuals of all ages can contract the virus, it poses a greater risk to older adults and those with pre-existing definite health conditions, such as diabetes, heart disease, or respiratory issues, see Adahoglu and Kaplan (2023), Aparecido Magrini et al. (2023); Pei and Liu (2023). By prioritizing these vulnerable groups, we can work towards a more inclusive and resilient public health approach that pays special attention to those who are most at risk. The analysis of stability and optimal control has been conducted on vaccination-implemented epidemic models, see Kar and Batabyal (2011); Sharma and Samanta (2015). Both studies enhance our understanding of the role of vaccination in controlling infectious diseases within the established model framework. A systematic review and meta-analysis reveal that proper vaccination significantly reduces the risk of SARS-CoV-2 infection, see Dinagde et al. (2024).

An evaluation of the epidemic system using a non-integer-order derivative has been presented in Butt et al. (2023) with the aim to achieve the most effective control possible over the pandemic's propagation. Insights into COVID-19 transmission dynamics, infection patterns, and control strategies in India are presented in Asker, Dhongde and Shonchoy (2025). The impact of the pandemic in four major European countries, with emphasis on changes in corporate financial behaviour during the crisis, is analyzed in Yaşar and Yalçin (2024). The impact of vaccination in Dougherty County, Georgia, USA, and its substantial contribution to epidemic control are demonstrated in Pantha, Mohammed-Awal and Vaidya (2022). A deterministic model for diphtheria transmission by Oguntolu et al. (2025) has been developed by incorporating the environmental concentration of Corynebacterium diphtheriae. A fractional-order model for drug-resistant HBV infection was developed, employing bifurcation and optimal control analyses to determine conditions for disease control and effective treatment strategies, by Teklu et al. (2025).

Recent epidemiological studies of COVID-19 have integrated vaccination and effective control measures to reduce community transmission across various countries, see Demongeot et al. (2022), González-Parra, Cogollo and Arenas (2022), Bai and Wang (2024), Lahrouz et al. (2012). Enhanced public health measures have reduced infections and boosted recoveries, raising community immunity, while mathematical modeling has supported stronger responses and

better surveillance. These strategies reduce infections and improve disease management, see Amaku et al. (2021), Xu et al. (2023), Tian et al. (2021), Bao and Hu (2023), Tegegn and Terefe (2025), Zhang et al. (2024). Such advancements equip public health organizations with the capacity to effectively address both present and emerging health issues. A dengue transmission model incorporating human awareness and behavioral responses was developed and calibrated using dengue case data from East Java, Indonesia, see Herdicho et al. (2025). An SIRUV model with human mobility was developed to study Mpox transmission, using parameter estimation and real data to design effective mobility-based interventions, see Hassan et al. (2025). A modelling study in Denmark showed that RSV causes excess mortality and hospitalisations comparable to influenza among older adults, see Egeskov-Cavling et al. (2025). Further investigations into pandemic control strategies, examining issues such as the adverse effects of quarantine on vulnerable groups, the dynamics of co-infections, and the effectiveness of various intervention approaches are presented in Kouidere et al. (2021), Bandekar and Gosh (2022), Castilho et al. (2020), Hu and Nie (2021), Choi and Shim (2021).

Leveraging the findings from the aforementioned research articles, our objective is to develop a robust epidemiological model that examines the dynamics of disease transmission while integrating effective control measures. This study specifically focuses on the progression of COVID-19 and aims to develop a pragmatic strategy for implementing more effective guidance in public health initiatives. From the reviewed studies, key research issues have been identified, which have to be addressed in order to improve understanding and control strategies of the epidemic model.

- Compared to linear assumptions, the Holling-type function provides a more realistic model by capturing the nonlinear pattern of infection transmission and regulation.
- Sensitivity index analysis selectively targets certain parameters within the epidemic model, focusing on key contributors to uncertainty rather than exhaustively evaluating all variables.
- Many infectious disease models are not validated with empirical data, which makes it difficult to assess the reliability of their parameter estimates. In this study, the model is developed with data-driven parameter estimation and is validated using observed data.
- The implementation of vaccination, treatment, and preventive measures offers important guidance for policymakers and healthcare professionals in controlling epidemic outbreaks.

To achieve this, we employ a mathematical framework that relies on categorization of the population into distinct groups: susceptible individuals, asymptomatic infectious carriers, symptomatic cases under quarantine, and those who

have recovered. Additionally, our model employs a non-monotonic incidence function to enhance its predictive accuracy and more effectively represent the complexities of the virus transmission.

2. Mathematical formulation

The proposed disease model is based on the assumed categorizations that are specific to the disease transmission context. Undiagnosed infected individuals can spread the disease, while those who have been identified are isolated should not contribute to transmission. The model is built on the following assumed categorization: susceptible individuals ($S(t)$) are currently healthy, but at risk of infection, while asymptomatic infected individuals ($I(t)$) are those infected with COVID-19 without exhibiting symptoms. Symptomatic infected individuals ($Q(t)$) show symptoms and receive treatment in quarantine. Recovered individuals ($R(t)$) are those who have recovered from asymptomatic (I) or symptomatic (Q) infection.

Numerous researchers have have been dealing with the nonlinear incidence rates, meaning to increase the comprehension of the dynamics in infectious disease models. For the SEIR and SIR models*, a non-monotonic incidence function was applied in the study by Wang, Zhang and Liu (2018); Ruan and Wang (2003). Here, we utilize the incidence function ($\frac{\gamma SI}{1+\mu I^2}$) to represent the spread of infection to the individuals, who are not showing the illness. The function describes disease transmission through the term γSI, while the factor $\frac{1}{1+\mu I^2}$ incorporates the effect of behavioral responses among susceptibles, which diminishes the infection rate as the infectious population grows.

The framework applies strategies to regulate system dynamics over time, utilizing three control variables to accomplish defined objectives. We have chosen the appropriate controls by using the references to the literature concerning the epidemic management of COVID-19, notably Omame, Isah and Abbas (2023), Chaharbojr et al. (2021), Zamir et al. (2021), Goswami et al. (2024). The control variable $h_1(t)$ pertains to personal protection measures, undertaken to prevent the transmission of the virus from infected persons who have no symptoms to those who are susceptible, see Nana-Kyere, Okyere and Ankamah (2020). These measures include social distancing, personal hygiene, face masks, and protective gear for healthcare professionals. The control variable $h_2(t)$ is related to the vaccination rate of susceptible individuals, excluding those who are already infected, see Kumar et al. (2022). Vaccination reduces the number of people at risk of infection and slows the spread of the disease. People, who have been vaccinated, develop an immune system in their bodies, although vaccination may not always provide complete protection against infection. The

*see the table of abbreviations at the end of the paper.

control variable $h_3(t)$ represents the treatment rate of symptomatic individuals, see Kumar et al. (2023). This formulation describes the system dynamics, subject to the influence of the control variables and sets the foundation for the mathematical model, presented below:

$$\begin{aligned}
\frac{dS}{dt} &= \varphi - (1 - h_1(t))\frac{\gamma SI}{1 + \mu I^2} - h_2(t)S - d_1 S, \\
\frac{dI}{dt} &= (1 - h_1(t))\frac{\gamma SI}{1 + \mu I^2} - \eta I - m_1 I - d_1 I, \\
\frac{dQ}{dt} &= \eta I - h_3(t)Q - d_2 Q, \\
\frac{dR}{dt} &= m_1 I + h_3(t)Q - d_1 R,
\end{aligned} \tag{2.1}$$

satisfying the initial conditions

$$S(0) = S_0 > 0,\ I(0) = I_0 > 0,\ Q(0) = Q_0 \geq 0, \text{ and } R(0) = R_0 \geq 0. \tag{2.2}$$

The choice of a non-monotonic incidence function is biologically motivated by the observation that, as infection levels rise, individuals tend to adopt preventive behaviors, already mentioned, such as social distancing, mask usage, and reduced contact rates. This behavioral feedback reduces effective transmission, making the non-monotonic formulation more realistic for modeling real-world epidemic scenarios compared to the classical bilinear incidence function.

A detailed explanation of each state variable is given in Table 1. All the variables are positive, and $W(t)$ is the total population of humans. The flow of virus transmission among humans is illustrated in Fig. 1. Pandemic uncertainty may increase stress levels and feelings of helplessness, raising concerns about health, financial security, and the future. In the proposed model, the inhibition effect is represented by μ, which prioritizes self-care for susceptible individuals. The model considers natural mortality rates (d_1) in the susceptibility, asymptomatic infection, and recovery compartments. Despite treatment, some individuals may not survive COVID-19. The notation d_2 represents the mortality rate, associated with the virus infection in the symptomatic individuals. The biological interpretations of the model parameters and control functions are presented in Tables 2 and 3, respectively.

To establish the fundamental dynamical properties of the system, we first analyze the model in the absence of time-varying interventions. For this dynamical analysis, the control functions are assumed to be constant and are specified as follows:

- $h_1(t) = 0$ (no transmission-reducing measures),
- $h_2(t) = 0$ (no vaccination of susceptibles),

- $h_3(t) = m_2$ (the recovery rate for quarantined individuals is constant).

This specification reduces the system to an autonomous one, allowing analysis of equilibrium points, stability, and the computation of the basic reproduction number $\Re_0$.

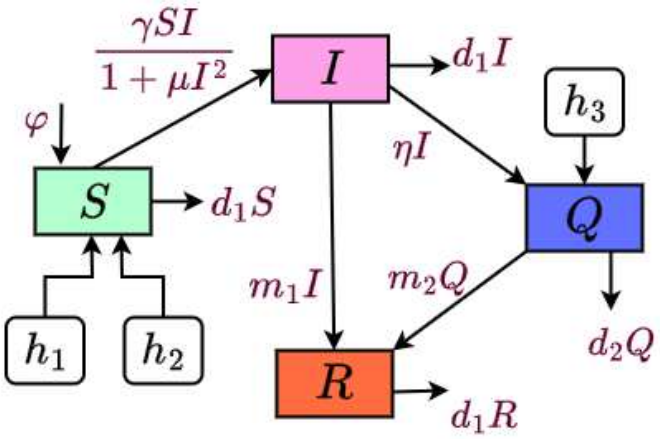

Figure 1: Schematic representation of virus spread in the human population with controls

Subsequently, for the optimal control analysis, the model is considered in its complete form with the time-dependent control functions $h_1(t)$, $h_2(t)$, and $h_3(t)$ as bounded, Lebesgue integrable functions. The objective is to determine an optimal strategy for deploying these controls over a fixed time interval to minimize the cost of disease burden and intervention efforts. This optimal control problem is analytically solved using Pontryagin's Maximum Principle (PMP), which provides the necessary conditions for optimality.

3. Well-posedness of the system

This section verifies the system's well-posedness by assuming that the time-dependent control functions h_1 and h_2 are absent and treating $h_3 = m_2$ as a constant parameter. We demonstrate the non-negativity and boundedness in the same contexts, and subsequently, derive equilibrium points and the corresponding basic reproduction number, which characterizes the threshold behavior and stability of the disease dynamics.

Table 1: State variables and their explanation

State variable	Explanation
$S(t)$	Individuals, who are susceptible to infection, but now remain in good condition
$I(t)$	Individuals, who have contracted the virus, but are not showing symptoms
$Q(t)$	Individuals, who are exhibiting symptoms of the virus and getting treatment in quarantine
$R(t)$	Individuals, who beat an infection, whether it was asymptomatic, I, or causing symptoms, Q

Table 2: Biological characteristics of model parameters

Parameter	Biological meaning	Unit
φ	Rate of recruitment of susceptible individuals	$\frac{1}{days}$
γ	Infection rate, at which susceptible individuals get sick without symptoms	$\frac{1}{days}$
μ	Parameter controlling the inhibitory effect of high infection on transmission	$\frac{1}{days}$
η	Rate, at which an illness transitions from asymptomatic to symptomatic	$\frac{1}{days}$
m_1	Asymptomatic infection recovery rate	$\frac{1}{days}$
m_2	Symptomatic infection recovery rate	$\frac{1}{days}$
d_1	Natural death rate among S, I and R individuals	$\frac{1}{days}$
d_2	Mortality rate caused by COVID-19 in people experiencing symptoms	$\frac{1}{days}$

Table 3: Control functions and their biological interpretation

Control function	Biological interpretation
$h_1(t)$	Effort to reduce disease transmission (e.g., masks, social distancing)
$h_2(t)$	Effort to vaccinate susceptible individuals
$h_3(t)$	Effort to treat quarantined individuals

3.1. Non-negativity of the solution

The non-negativity of solutions of the system of Eq. (2.1) is established under the initial conditions of Eq. (2.2). Also, the boundedness of the system is determined in the invariant region.

Theorem 1 *For each time $t > 0$, the set of equations of Eq. (2.1) has non-negative solutions with respect to the initial conditions, established in Eq. (2.2).*

Proof By utilizing the first equation from the set of Eq. (2.1),

$$\frac{dS}{dt} = \varphi - \frac{\gamma SI}{1+\mu I^2} - d_1 S,$$

we derive the subsequent inequality:

$$\frac{dS}{dt} > \left(-\frac{\gamma I}{1+\mu I^2} - d_1\right) S.$$

By integrating, we find the following:

$$S(t) > S(0)e^{-\int_0^t \phi(I(x))dx}, \text{ where } \phi(I(x)) = \left(\frac{\gamma I(x)}{1+\mu I^2(x)} + d_1\right).$$

Consequently, since $S(0) > 0$, $S(t)$ remains non negative for all times $t > 0$.

From the second equation of the system of Eq. (2.1),

$$\frac{dI}{dt} = \frac{\gamma SI}{1+\mu I^2} - \eta I - m_1 I - d_1 I.$$

Since $\frac{\gamma SI}{1+\mu I^2} \geq 0$, we obtain

$$\frac{dI}{dt} \geq -\eta I - m_1 I - d_1 I.$$

Upon letting $k_1 = \eta + m_1 + d_1$, we deduce that $I(t) \geq I(0)e^{-k_1 t} \geq 0$, for $I(0) > 0$. Hence, $I(t)$ remains nonnegative for all $t > 0$.

Similarly, considering the third equation of Eq. (2.1),

$$\frac{dQ}{dt} = \eta I - m_2 Q - d_2 Q.$$

Since $\eta I \geq 0$, we obtain

$$\frac{dQ}{dt} \geq -m_2 Q - d_2 Q.$$

Because $Q(0) \geq 0$, it follows that $Q(t) \geq Q(0)e^{-k_2 t} \geq 0$, where $k_2 = m_2 + d_2$. Thus, $Q(t)$ remains nonnegative for all $t > 0$. Finally, for the last equation,

$$\frac{dR}{dt} = m_1 I + m_2 Q - d_1 R.$$

Since $m_1 I + m_2 Q \geq 0$, it follows that

$$\frac{dR}{dt} \geq -d_1 R.$$

Therefore, the solution satisfies $R(t) \geq R(0)e^{-d_1 t} \geq 0$ with the initial condition $R(0) \geq 0$.

Hence, under the initial conditions of Eq. (2.2), all the solutions remain positive for every $t > 0$. ∎

3.2. Boundedness and invariant region

THEOREM 2 *The system's solutions residing within $\mathbb{R}^4_+$, are uniformly bounded and limited to the invariant region $\Omega = \{(S, I, Q, R) \in \mathbb{R}^4_+ : 0 < W(t) \leq \frac{\varphi}{u}\}$ as $t \to \infty$, where $u = \min\{d_1, d_2\}$.*

PROOF The total population's rate of change over time is provided by

$$\frac{dW(t)}{dt} = \varphi - (d_1 S + d_1 I + d_2 Q + d_1 R).$$

Introduction of a positive constant u and rearrangement of the equation, yields

$$\frac{dW(t)}{dt} + uW = \varphi - (d_1 - u)S - (d_1 - u)I - (d_2 - u)Q - (d_1 - u)R.$$

Setting $u = \min\{d_1, d_2\}$, gives $\frac{dW(t)}{dt} + uW \leq \varphi$. To derive the solution, we can proceed as follows:

$$0 < W(t) \leq \frac{\varphi}{u}(1 - e^{-ut}) + W(0)e^{-ut}.$$

As $t \to \infty$, we have the solution $0 < W(t) \leq \frac{\varphi}{u}$. Therefore, solutions starting from the initial conditions of Eq. (2.2) within $\mathbb{R}^4_+$ are uniformly bounded and limited to the region

$$\Omega = \{(S, I, Q, R) \in \mathbb{R}^4_+ : 0 < W(t) \leq \frac{\varphi}{u}; u = \min\{d_1, d_2\}\}.$$

Therefore, as a positively invariant set, Ω additionally includes uniformly bounded solutions. ■

From a mathematical and biological perspective, the model represented by Eq. (2.1) is well-posed under the initial conditions within the region Ω. Together, these basic properties of the model ensure that it provides a realistic and biologically plausible representation of COVID-19 dynamics, keeping the population states within meaningful bounds and accurately reflecting the natural constraints of disease transmission and population dynamics.

3.3. Equilibrium points and the BRN

The epidemic model's equilibrium points are the disease-free equilibrium (DFE), where no infection occurs in the entire population, and the endemic equilibrium (EE), where infection remains at a constant level in the overall population. BRN is the mean number of additional infections, resulting from an individual case of a disease.

(i)The DFE point is given by $N^0(S^0, I^0, Q^0, R^0)$, where $S^0 = \frac{\varphi}{d_1}$, $I^0 = 0$, $Q^0 = 0$, and $R^0 = 0$.

To determine the BRN, the dynamical model of Eq. (2.1) is subjected to the next generation matrix method (NGM), see Van der Driessche and Watmough (2002). It is a significant numerical threshold that provides insight into the potential spread of a viral infection. Let $z = (I, Q, R, S)^T$; then, the system of equation Eq. (2.1) can be formulated as $\dfrac{dz}{dt} = \mathcal{F} - \mathcal{V}$, where

$$\mathcal{F}(z) = \begin{bmatrix} \frac{\gamma SI}{1+\mu I^2} \\ 0 \\ 0 \\ 0 \end{bmatrix} \text{ and } \mathcal{V}(z) = \begin{bmatrix} k_1 I \\ -\eta I + k_2 Q \\ -m_1 I - m_2 Q + d_1 R \\ -\varphi + \frac{\gamma SI}{1+\mu I^2} + d_1 S \end{bmatrix}.$$

At the DFE point N^0, we have

$$F = \begin{bmatrix} \frac{\gamma\varphi}{d_1} & 0 & 0 & 0 \\ 0 & 0 & 0 & 0 \\ 0 & 0 & 0 & 0 \\ 0 & 0 & 0 & 0 \end{bmatrix} \text{ and } V = \begin{bmatrix} k_1 & 0 & 0 & 0 \\ -\eta & k_2 & 0 & 0 \\ -m_1 & -m_2 & d_1 & 0 \\ \frac{\gamma\varphi}{d_1} & 0 & 0 & d_1 \end{bmatrix}.$$

After computation, the NGM becomes $FV^{-1} = \begin{bmatrix} \frac{\gamma\varphi}{d_1 k_1} & 0 & 0 & 0 \\ 0 & 0 & 0 & 0 \\ 0 & 0 & 0 & 0 \\ 0 & 0 & 0 & 0 \end{bmatrix}$.

Therefore, the spectral radius of the NGM at the DFE point N^0 is the BRN for the system of Eq. (2.1), which is denoted by $\Re_0 = \frac{\gamma\varphi}{d_1 k_1}$.

(ii) In order to determine, whether the system in Eq. (2.1) has a nontrivial EE, let $S > 0$, $I > 0$, $Q > 0$, $R > 0$ and $\frac{dS}{dt} = \frac{dI}{dt} = \frac{dQ}{dt} = \frac{dR}{dt} = 0$. Using the last two nullclines and solving for Q and R, the following expressions

$$Q^* = \frac{\eta I^*}{k_2},\ R^* = \frac{(k_2 m_1 + \eta m_2) I^*}{d_1 k_2}$$

are obtained.

The following is the result of utilizing the second nullcline and Q^* and R^* to obtain $S^* = \dfrac{k_1 + I^{*2} k_1 \mu}{\gamma}$.

Using S^*, Q^*, and R^* in the first nullcline, a fourth-degree polynomial in I^* is obtained as follows:

$$I^{*4} + \alpha_1 I^{*3} + \alpha_2 I^{*2} + \alpha_3 I^* + \alpha_4 = 0,$$

with

$$\alpha_1 = \frac{\gamma}{d_1 \mu},\ \alpha_2 = \frac{2 d_1 k_1 - \gamma\varphi}{d_1 k_1 \mu},\ \alpha_3 = \frac{\gamma}{d_1 \mu^2},\ \text{and}\ \alpha_4 = \frac{d_1 k_1 - \gamma\varphi}{d_1 k_1 \mu^2} = \frac{1 - \Re_0}{\mu^2}.$$

According to Descartes's rule, the polynomial has at least one positive root if and only if $\Re_0 > 1$. Thus, the EE point $N^*(S^*, I^*, Q^*, R^*)$ occurs if and only if $\Re_0 > 1$.

3.4. Stability assessment of equilibrium

To examine the behavior of the system in proximity to the equilibrium points, this method involves the generation of the Jacobian matrix and the examination of its eigenvalues. The Jacobian matrix can be evaluated for the given system of Eq. (2.1) as follows:

$$J = \begin{bmatrix} -\frac{\gamma I}{1+\mu I^2} - d_1 & -\frac{\gamma S(1-\mu I^2)}{(1+\mu I^2)^2} & 0 & 0 \\ \frac{\gamma I}{1+\mu I^2} & \frac{\gamma S(1-\mu I^2)}{(1+\mu I^2)^2} - k_1 & 0 & 0 \\ 0 & \eta & -k_2 & 0 \\ 0 & m_1 & m_2 & -d_1 \end{bmatrix}.$$

Local behavior of DFE and EE:

THEOREM 3 *The DFE $N^0(S^0, I^0, Q^0, R^0)$ of the system of Eq. (2.1) is LAS for $\Re_0 < 1$ and is unstable for $\Re_0 > 1$.*

Proof At DFE point $N^0(S^0, I^0, Q^0, R^0)$, the Eq. (2.1) system's Jacobian matrix $J(N^0)$ can be written as

$$J(N^0) = \begin{bmatrix} -d_1 & -\frac{\gamma\varphi}{d_1} & 0 & 0 \\ 0 & \frac{\gamma\varphi}{d_1} - k_1 & 0 & 0 \\ 0 & \eta & -k_2 & 0 \\ 0 & m_1 & m_2 & -d_1 \end{bmatrix}.$$

The characteristic polynomial $|J(N^0) - \lambda I| = 0$ is expressed as

$$|J(N^0) - \lambda I| = \begin{vmatrix} -d_1 - \lambda & -\frac{\gamma\varphi}{d_1} & 0 & 0 \\ 0 & \frac{\gamma\varphi}{d_1} - k_1 - \lambda & 0 & 0 \\ 0 & \eta & -k_2 - \lambda & 0 \\ 0 & m_1 & m_2 & -d_1 - \lambda \end{vmatrix}.$$

Solution of the characteristic polynomial gives the characteristic roots of the matrix

$$J(N^0) : \lambda_1 = -d_1,\ \lambda_2 = -d_1,\ \lambda_3 = -k_2, \lambda_4 = -k_1(1 - \frac{\gamma\varphi}{d_1 k_1}) = -k_1(1 - \Re_0).$$

The first three roots are clearly negative, while the last root becomes negative if $\Re_0 < 1$ and turns positive when $\Re_0 > 1$. According to the Hurwitz-Routh Criterion, see Yildiz et al. (2022), the DFE point N^0 is therefore an LAS when $\Re_0 < 1$. Furthermore, the DFE point N^0 is unstable for $\Re_0 > 1$. ∎

Theorem 4 *If all the conditions established in the proof are satisfied and the BRN $\Re_0$ exceeds 1, then the endemic equilibrium point N^* of the model in Eq.(2.1) is locally asymptotically stable within the feasible region Ω.*

Proof At the EE point N^*, the Jacobian matrix of the system of Eq.(2.1) becomes,

$$J = \begin{pmatrix} -\frac{\gamma I^*}{1+\mu I^{*2}} - d_1 & -\frac{\gamma S^*(1-\mu I^{*2})}{(1+\mu I^{*2})^2} & 0 & 0 \\ \frac{\gamma I^*}{1+\mu I^{*2}} & \frac{\gamma S^*(1-\mu I^{*2})}{(1+\mu I^{*2})^2} - k_1 & 0 & 0 \\ 0 & \eta & -k_2 & 0 \\ 0 & m_1 & m_2 & -d_1 \end{pmatrix}$$

The above matrix can be expressed as $|J(N^*) - \lambda I| = 0$. We have,

$$(\lambda + d_1)(\lambda + k_2) P(\lambda) = 0,$$

where

$$P(\lambda) = \lambda^2 + b_1\lambda + b_2. \tag{3.1}$$

The obtained two roots of the characteristic polynomial are $\lambda = -d_1 < 0$ and $\lambda = -k_2 < 0$. To analyze further roots, we obtain the coefficients of Eq.(3.1) as follows:

$$b_1 = \frac{d_1 S^* \gamma(-1 + {I^*}^2\mu) + I^* k_1 \gamma(1 + {I^*}^2\mu) + d_1 k_1 (1 + {I^*}^2\mu)^2}{(1 + {I^*}^2\mu)^2},$$

$$b_2 = \frac{d_1 + k_1 + I^*\gamma - S^*\gamma + {I^*}^2 \left(2(d_1 + k_1) + (I^* + S^*)\gamma\right)\mu + {I^*}^4 (d_1 + k_1)\mu^2}{(1 + {I^*}^2\mu)^2}.$$

In the case of a second-order polynomial, the Hurwitz-Routh criterion states that all roots possess negative real parts if and only if the following constraints are satisfied: $b_i > 0$, $i = 1, 2$. However, the EE point N^* exists in Ω if $\Re_0 > 1$. Under these conditions, N^* is an LAS in Ω. ■

Global behavior of DFE:

The GAS of N^0 is analyzed in this section using the CCM, see Castillo-Chavez et al. (2002), based on the value of $\Re_0$ in the feasible region $\Omega_1 = \{(S, I, Q, R) \in \Omega : S \leq S^0\}$. First, the property of being positively invariant for the region Ω_1 is proven.

THEOREM 5 *The set $\Omega_1 = \{(S, I, Q, R) \in \Omega : S \leq S^0\}$ exhibits the property of positive invariance for the system in Eq. (2.1).*

PROOF By considering the system of Eq. (2.1), the inequality $\frac{dS}{dt} = \varphi - \frac{\gamma SI}{1+\mu I^2} - d_1 S \leq \varphi - d_1 S$ is derived. If $S(0) \in \Omega_1$, then $S(0) \leq S^0$. Hence,

$$S(t) \leq -(S^0 - S(0))e^{-d_1 t} + \frac{\varphi}{d_1} \leq \frac{\varphi}{d_1} = S^0,$$

when the initial condition satisfies $S(0) \in \Omega_1$. Therefore, for all $t \geq 0$, the variable $S(t)$ remains bounded by S^0. Consequently, the solution of the model of Eq. (2.1) in $\mathbb{R}^4_+$ is attracted to the positively invariant set Ω_1, establishing it as a region that retains its properties over time. ■

THEOREM 6 *If $\Re_0 < 1$, DFE N^0 is GAS in Ω_1.*

PROOF The given system of Eq. (2.1) is defined as follows, see Omorogie, Owolabi and Olabode (2014):

$$\dot{\epsilon} = K(\epsilon, \zeta), \ \dot{\zeta} = L(\epsilon, \zeta). \tag{3.2}$$

Here, $\dot{\epsilon}$ and $\dot{\zeta}$ symbolize the derivatives of ϵ and ζ, respectively, with regard to t. We have $\epsilon = (S, R)^T$, and $\zeta = (I, Q)^T$. Then, we obtain

$$K(\epsilon, \zeta) = \begin{pmatrix} \varphi - \frac{\gamma SI}{1+\mu I^2} - d_1 S \\ m_1 I + m_2 Q - d_1 R \end{pmatrix}, \qquad L(\epsilon, \zeta) = \begin{pmatrix} \frac{\gamma SI}{1+\mu I^2} - k_1 I \\ \eta I - k_2 Q \end{pmatrix}.$$

Furthermore, from Tchoumi, Schwartz and Tchuenche (2024), we have

$$A = \begin{pmatrix} \frac{\gamma\varphi}{d_1} & 0 \\ \eta & -k_2 \end{pmatrix}, \quad \hat{L}(\epsilon,\zeta) = \begin{pmatrix} [\gamma(S^0 - S) + k_1]I \\ 0 \end{pmatrix},$$

$$K(\epsilon,\zeta)\Big|_{I=0} = \begin{pmatrix} \varphi - d_1 S \\ -d_1 R \end{pmatrix}, \quad L(\epsilon,\zeta)\Big|_{I=0} = \begin{pmatrix} 0 \\ 0 \end{pmatrix},$$

where $A = D_I L(\epsilon^*, 0)$, and $L(\epsilon,\zeta) = AI - \hat{L}(\epsilon,\zeta)$.

By solving the system $\frac{d\epsilon}{dt} = K(\epsilon, 0)$, we obtain $S(t) = S^0 + (S(0) - S^0)e^{-d_1 t}$, and hence $\lim_{t\to\infty} S(t) = S^0$; similarly, from the other equation of $\frac{d\epsilon}{dt} = K(\epsilon, 0)$, which yields $\lim_{t\to\infty} R(t) = R^0$. Therefore, the solutions of the differential equation $\frac{d\epsilon}{dt} = K(\epsilon, 0)$ are independent of the initial conditions ($S(0)$, $R(0)$). The asymptotic character of the solutions ($S(t)$, $R(t)$) is also independent of the initial conditions in Ω_1, ensuring that the GAS of the equilibrium point $N^0 = (S^0, I^0, Q^0, R^0) = (\frac{\varphi}{d_1}, 0, 0, 0)$. Hence, the first condition of the CCM is satisfied. Furthermore, in Ω_1, $S \leq S^0$; hence, $[\gamma(S^0 - S) + k_1] \geq 0$. This indicates that $\hat{L}(\epsilon,\zeta) \geq 0$, which fulfills the second requirement. As a result, N^0 is the GAS if $\Re_0 < 1$. ∎

4. Bifurcation analysis

A brief bifurcation analysis is carried out to understand how the system transitions between the disease-free and endemic states as key parameters vary. The model exhibits a forward bifurcation, demonstrating the smooth emergence of a stable endemic equilibrium once the threshold condition is crossed.

Theorem 7 *The system of Eq. (2.1) experiences forward bifurcation at* $\Re_0 = 1$.

Proof Let $S = x_1$, $I = x_2$, $Q = x_3$, and $R = x_4$. Then, the model of Eq. (2.1) becomes

$$\dot{x}_1 = \varphi - \frac{\gamma x_1 x_2}{1 + \mu x_2^2} - d_1 x_1 = f_1,$$

$$\dot{x}_2 = \frac{\gamma x_1 x_2}{1 + \mu x_2^2} - \eta x_2 - m_1 x_2 - d_1 x_2 = f_2,$$

$$\dot{x}_3 = \eta x_2 - m_2 x_3 - d_2 x_3 = f_3,$$

$$\dot{x}_4 = m_1 x_2 + m_2 x_3 - d_1 x_4 = f_4.$$

Consider the bifurcation parameter γ, the infection rate at which susceptible individuals become sick without symptoms. When $\Re_0 = 1$, the critical point

is represented as $\gamma^* = \frac{d_1 k_1}{\varphi}, k_1 = \eta + m_1 + d_1$. The DFE point is given by $N^0(x_1^0, x_2^0, x_3^0, x_4^0)$, where $x_1^0 = \frac{\varphi}{d_1}$, $x_2^0 = 0$, $x_3^0 = 0$, $x_4^0 = 0$. The Jacobian matrix J at the DFE point N^0 is determined as

$$J(N^0) = \begin{bmatrix} -d_1 & -\frac{\gamma\varphi}{d_1} & 0 & 0 \\ 0 & \frac{\gamma\varphi}{d_1} - k_1 & 0 & 0 \\ 0 & \eta & -k_2 & 0 \\ 0 & m_1 & m_2 & -d_1 \end{bmatrix}.$$

We simplify by setting $\frac{\gamma\varphi}{d_1} = k_1$, which results in the Jacobian matrix, expressed as

$$J(N^0) = \begin{bmatrix} -d_1 & -k_1 & 0 & 0 \\ 0 & 0 & 0 & 0 \\ 0 & \eta & -k_2 & 0 \\ 0 & m_1 & m_2 & -d_1 \end{bmatrix}.$$

To find the right eigenvector $\mathbf{w} = (w_1, w_2, w_3, w_4)^T$, solving $J(N^0).\mathbf{w} = \mathbf{0}$, we obtain the right eigenvector

$$\mathbf{w} = \left(-\frac{k_1}{d_1} w_2, w_2, \frac{\eta}{k_2} w_2, \frac{m_1 k_2 + m_2 \eta}{d_1 k_2} w_2 \right)^T.$$

The left eigenvector $\mathbf{v} = (v_1, v_2, v_3, v_4)^T$ must satisfy $\mathbf{v}^T.J(N^0) = 0$. Solving this, we find $v_1 = 0$ and $v_4 = 0$. Additionally, the conditions imply that $v_3 = 0$. Thus, the left eigenvector can be expressed in terms of v_2 as: $\mathbf{v} = (0, v_2, 0, 0)^T$, where v_2 is a free parameter. To find the components of the left eigenvector $\mathbf{v}$, we use the normalization condition $\mathbf{v}^T\mathbf{w} = 1$. Consequently, the final forms of the eigenvectors are $\mathbf{w} = w_2 \begin{pmatrix} -\frac{k_1}{d_1} & 1 & \frac{\eta}{k_2} & \frac{m_1 k_2 + m_2 \eta}{d_1 k_2} \end{pmatrix}^T$, and $\mathbf{v} = \begin{pmatrix} 0 & \frac{1}{w_2} & 0 & 0 \end{pmatrix}^T$. The bifurcation coefficients are given by

$$a = \sum_{k,i,j=1}^{4} v_k w_i w_j \frac{\partial^2 f_k(N^0, \gamma^*)}{\partial x_i \partial x_j},$$

$$b = \sum_{k,i,j=1}^{4} v_k w_i \frac{\partial^2 f_k(N^0, \gamma^*)}{\partial x_i \partial \gamma}.$$

After simplification, we obtain the bifurcation coefficients

$$a = -\frac{2(d_1 + m_1 + \eta)^2 w_2}{\varphi}$$

and

$$b = \frac{\varphi}{d_1}.$$

If it is assumed that $w_2 > 0$, then $a < 0$; otherwise, $a > 0$.

This combination of $a < 0$ and $b > 0$ corresponds to *forward bifurcation*, meaning that the system undergoes a smooth switch from DFE to EE as the bifurcation parameter crosses a critical threshold, see Cheng and Qiao (2025). Biologically, this means that once the disease becomes established in the population, it settles into a steady endemic level and does not disappear on its own. This type of bifurcation indicates that controlling the disease after this point becomes difficult, as the system naturally remains in an endemic state. ■

Figure 2 clearly illustrates the transition, bifurcation point, with the stable endemic state branching out from the unstable disease-free state, thus confirming forward bifurcation.

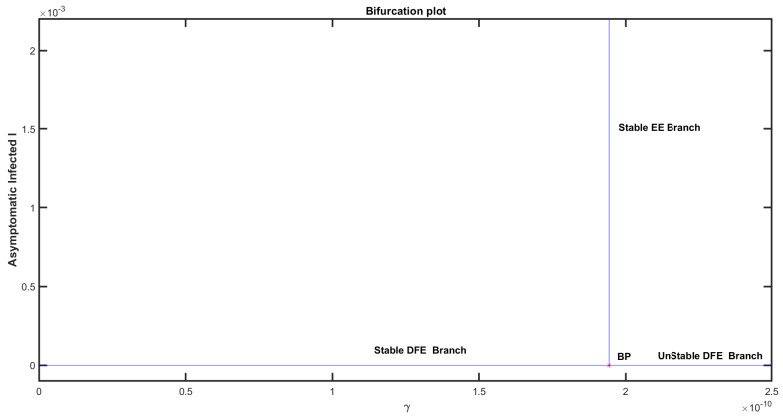

Figure 2: Bifurcation plot at $\Re_0 = 1$ for infected population

The study explores how the infected population (I) responds by varying the parameter γ, focusing on the transition at the threshold $\Re_0 = 1$. Using MATCONT, the bifurcation parameter γ was systematically varied, and a forward bifurcation was observed, as shown in Fig. 2 using parameter values, provided in Table 6. This phenomenon was theoretically anticipated and analytically verified in a previous theorem. At the critical value of $\gamma = 1.9430 \times 10^{-10}$, corresponding to $\Re_0 = 1$, the DFE becomes unstable and EE emerges.

Table 4: Estimated parameter values for three countries

Parameter	Afghanistan	Austria	Brazil
φ	8.04×10^{4}	7.26×10^{5}	7.85×10^{7}
γ	2.9×10^{-10}	3.22×10^{-10}	2.37×10^{-11}
μ	2.02×10^{-16}	4.32×10^{-14}	2.05×10^{-13}
η	0.20	0.23	0.35
m_1	0.13	0.22	0.005
m_2	0.11	0.07	0.05
d_1	6.02×10^{-5}	6.95×10^{-18}	6.33×10^{-18}
d_2	0.0003	0.001	8.64×10^{-17}

5. Parameter estimation and model validation

In this section, we apply the model to examine the dynamics of COVID-19 transmission across three countries. Parameter estimation is a crucial step in mathematical modeling, involving the adjustment of model parameters to fit the real data. Subsequent validation of the model revealed strong agreement between the estimated parameters and the actual disease trends. In this study, we utilized real-time infected case data, see Mathieu et al. (2020), for three countries, Afghanistan (22 July 2020 to 18 February 2023, 941 days), Austria (28 August 2021 to 22 June 2022, 301 days), and Brazil (5 January 2020 to 4 August 2024, 1664 days), and fitted the model symptomatic infected population Q, as shown in Fig. 3.

We used the Simulink Parameter Estimation tool to estimate key biological parameters (Table 4) for the model, including the human recruitment rate (φ), infection rate (γ), rate of symptom development (η), and recovery rates for asymptomatic and symptomatic individuals (m_1 and m_2, respectively). Each unique epidemic trend requires adjusting the parameter values to accurately reflect local transmission dynamics. For example, Brazil's large dataset demonstrated the model's robustness over time, showing excellent validation even with extended periods of data. This suggests that the parameter estimation process is reliable and flexible for both short and long-term epidemic patterns.

In conclusion, parameter estimation and model validation definitely significantly improve the reliability and predictive capacity of infectious disease models. This process not only enhances the accuracy of the model, but also offers biological insights into disease progression, recovery, and mortality. Future research should focus on extending these models to other regions and incorporating new data to improve predictions and further inform public health strategies.

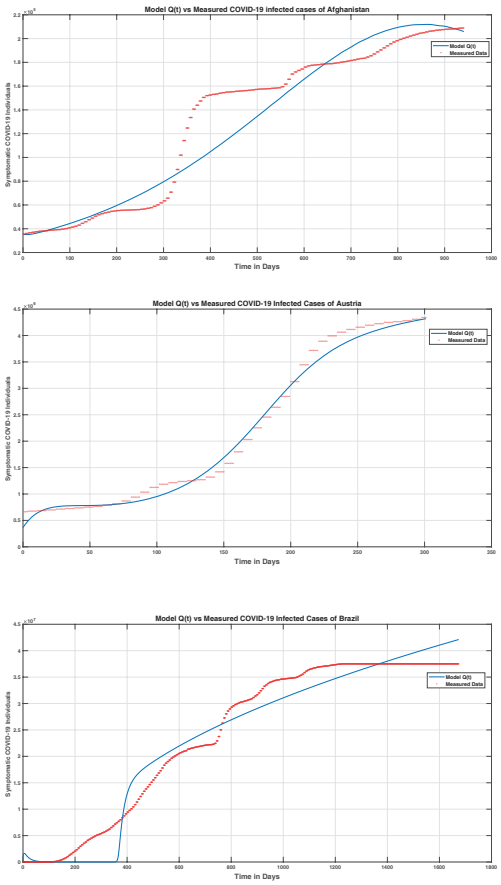

Figure 3: Model validation of three countries using real infected cases

6. Sensitivity analysis

The *normalized forward sensitivity index* (NFSI) is utilized to carry out the sensitivity analysis of the BRN, which is denoted as $\Re_0$. The NFSI measures the sensitivity of $\Re_0$ to changes in the model parameters and is defined as: $\Gamma_m^{\Re_0} = \dfrac{\partial \Re_0}{\partial m} \dfrac{m}{\Re_0}$, where m represents a model parameter. The NFSI values for each parameter are calculated as this is shown in Table 5.

The analysis revealed that the parameters φ (recruitment rate of individuals susceptible to infection) and γ (infection rate at which susceptible individuals become sick without symptoms) have a positive influence on the transmission

Table 5: NFSI of $\Re_0$ relative to model parameters

Parameter	NFSI of $\Re_0$
φ	1
γ	1
d_1	$-1-\frac{d_1}{\eta+m_1+d_1}$
η	$-\frac{\eta}{\eta+m_1+d_1}$
m_1	$-\frac{m_1}{\eta+m_1+d_1}$

of the virus, as indicated by their positive NFSI values. In contrast, the parameters d_1 (the natural death rate for individuals), η (the rate of symptom progression), and m_1 (the rate of recovery from asymptomatic infection) negatively influence disease spread, as indicated by their negative NFSI values. Parameters μ, m_2, and d_2 do not affect $\Re_0$. Essential elements in managing the spread of COVID-19 can be identified by recognizing the sensitivity of $\Re_0$ to various parameters. Interventions that reduce γ (e.g., improving the isolation of asymptomatic cases and reducing contact rates) or increase η and m_1 (e.g., enhancing the detection and treatment rates of asymptomatic cases) effectively reduce the spread. Public health authorities can focus on these areas for targeted interventions. Additionally, measures that do not significantly impact $\Re_0$ (such as those affecting μ, m_2, and d_2) may be deprioritized in favor of more impactful strategies. By focusing on parameters with the highest sensitivity, resources can be allocated to maximize the reduction in disease transmission, ultimately assisting policymakers in designing effective intervention strategies for controlling the pandemic.

7. Optimal control strategies

7.1. The setting

In this section, we analyze the model of Eq. (2.1) that includes time-dependent control functions for the purpose of investigating the optimal control strategy. The following provides the objective function:

$$J(h_1(t), h_2(t), h_3(t)) = \int_0^{t_f} \left[C_1 I + C_2 h_1^2 + C_3 h_2^2 + C_4 h_3^2\right] \, dt,$$

where C_i for $i = 1, 2, 3, 4$ are weight factors used in the cost function. The objective is to decrease the overall number of individuals exposed or infected, in addition to reducing the associated costs related to the implementation of protective measures, vaccinations, and treatments. Since the symptomatic infected population in a quarantined period (Q) does not contribute to disease transmission, it is excluded from the objective function $J(h_1(t), h_2(t), h_3(t))$. The purpose is to determine the set of control functions (h_1^*, h_2^*, h_3^*) that optimize the objective function, see Ben Cherif, Balatif and Kabiri (2024):

$$J(h_1^*, h_2^*, h_3^*) = \min\{J(h_1, h_2, h_3) : (h_1, h_2, h_3) \in U_h\}.$$

The set of admissible controls is defined as

$$U_h = \{(h_1, h_2, h_3) : h_1, h_2, h_3 \text{ are measurable functions}, 0 \leq h_1, h_2, h_3 \leq 1\}$$

and t ranges from 0 to t_f. In optimal control theory, the PMP can be applied to determine an effective control approach that minimizes the objective function while adhering to system dynamics and constraints. The resulting optimal control measures can guide decision-making for effective intervention strategies in managing the spread of disease.

7.2. Optimal control existence

Theorem 8 *For the system of Eq. (2.1) with initial conditions of Eq.* (2.2), $\exists$ *a set* (h_1^*, h_2^*, h_3^*) *such that* $J(h_1^*, h_2^*, h_3^*) = \min\{J(h_1, h_2, h_3) : (h_1, h_2, h_3) \in U_h\}$ *attains a minimum value. This optimal control set is obtained from* $U_h = \{(h_1, h_2, h_3) : h_1, h_2, h_3$ *are measurable functions*$, 0 \leq h_1, h_2, h_3 \leq 1\}$ *and* t *ranging from 0 to* t_f.

Proof The results from Ma et al. (2023), De Oliveira et al. (2023) can be applied to show the optimum control existence. A linear system clearly bounds the system of Eq. (2.1). The boundedness of the system of Eq. (2.1) solutions over time is employed to show that there is optimum control. First, we analyze the subsequent characteristics:

(a) The control function in the set and the related Eq. (2.1) system's solution set is nonempty.
(b) The control set U_h is convex and closed.
(c) The right hand side of the system in Eq. (2.1) is bounded by a linear function.
(d) The integrand of $J(h_1(t), h_2(t), h_3(t))$ is convex on U_h.
(e) $\exists$ constants $l_1, l_2 > 0$ and $q > 1$, $\ni C_1 I + C_2 h_1^2 + C_3 h_2^2 + C_4 h_3^2$ fulfills the condition $C_1 I + C_2 h_1^2 + C_3 h_2^2 + C_4 h_3^2 \geq l_1(\sum_{i=1}^{3} |h_i|^2)^{\frac{q}{2}} + l_2$.

The first requirement is that the control set, defined as U_h, along with the states, must be nonempty. This gives condition (b) since the control set $(h_1, h_2, h_3)(t)$ is closed and convex from the definition. Because the solutions are a priori limited, the state system of Eq. (2.1) on the right-hand side follows the condition (c). The integrand in the objective function, $C_1 I + C_2 h_1^2 + C_3 h_2^2 + C_4 h_3^2$ is clearly convex on U_h. For some positive values $l_1, l_2 > 0$, and $q > 1$, the objective function is $J \geq l_1(|h_1|^2 + |h_2|^2 + |h_3|^2)^{\frac{q}{2}} + l_2$. Based on the requirements, there exists an optimal control set $(h_1^*, h_2^*, h_3^*)(t)$, which minimizes the objective function J. ∎

Description of the optimal triple of controls:

By PMP, Lagrangian L can be framed as,

$$L(I, h_1, h_2, h_3) = C_1 I + C_2 h_1^2 + C_3 h_2^2 + C_4 h_3^2,$$

and H represents the Hamiltonian

$$H(S, I, Q, R, h_1, h_2, h_3, \delta_i, t) = L(I, h_1, h_2, h_3) + \sum_{i=1}^{4} \delta_i g_i.$$

The variables $g_1,\ g_2,\ g_3$, and g_4 represent the right hand side of the equation Eq. (2.1), whereas $\delta_1(t),\ \delta_2(t),\ \delta_3(t)$, and $\delta_4(t)$ refer to adjoint functions, which are related to the system of equations, and whose values are to be determined appropriately.

$$\begin{aligned} H = {} & C_1 I + C_2 h_1^2 + C_3 h_2^2 + C_4 h_3^2 + \delta_1 \Big(\varphi - (1 - h_1(t)) \frac{\gamma S I}{1 + \mu I^2} - h_2(t) S - d_1 S\Big) \\ & + \delta_2 \Big((1 - h_1(t)) \frac{\gamma S I}{1 + \mu I^2} - \eta I - m_1 I - d_1 I\Big) + \delta_3 \Big(\eta I - h_3(t) Q - d_2 Q\Big) \\ & + \delta_4 \Big(m_1 I + h_3(t) Q - d_1 R\Big). \end{aligned} \tag{7.1}$$

The transversality requirements and the form of the adjoint equations are conventional effects of PMP. The following is the process used to acquire the adjoint system:

$$\frac{\partial \delta_1}{\partial t} = -\frac{\partial H}{\partial S} = (d_1 + h_2)\delta_1 - \frac{(-1 + h_1) I \gamma (\delta_1 - \delta_2)}{1 + I^2 \mu}$$

$$\begin{aligned} \frac{\partial \delta_2}{\partial t} = -\frac{\partial H}{\partial I} = {} & -C_1 + (d_1 + m_1 + \eta)\delta_2 - m_1 \delta_4 - \delta_3 \eta \\ & + \frac{(-1 + h_1) S \gamma (\delta_1 - \delta_2)(-1 + I^2 \mu)}{(1 + I^2 \mu)^2} \end{aligned}$$

$$\frac{\partial \delta_3}{\partial t} = -\frac{\partial H}{\partial Q} = (d_2 + h_3)\delta_3 - h_3\delta_4$$

$$\frac{\partial \delta_4}{\partial t} = -\frac{\partial H}{\partial R} = d_1\delta_4$$

with the transversality condition $\delta_1(t_f) = \delta_2(t_f) = \delta_3(t_f) = \delta_4(t_f) = 0$. Based on the optimality criterion and together with $\frac{\partial H}{\partial h_i} = 0$, at $h_i^*(t), i = 1, 2, 3$, we obtain

$$h_1^*(t) = \frac{I^* S^* \gamma(\delta_1 - \delta_2)}{2C_2(1 + I^{*2}\mu)},\ h_2^*(t) = \frac{S^*\delta_1}{2C_3},\ \text{and}\ h_3^*(t) = \frac{Q(\delta_3 - \delta_4)}{2C_4}.$$

As the maxima and minima are given by the bounds, we can characterize the optimal control in the following way, see Abbasi et al. (2020):

$$h_1^* = \min\left\{\max\left(0, \frac{I^* S^* \gamma(\delta_1 - \delta_2)}{2C_2(1 + I^{*2}\mu)}\right), 1\right\},$$

$$h_2^* = \min\left\{\max\left(0, \frac{S^*\delta_1}{2C_3}\right), 1\right\},$$

$$h_3^* = \min\left\{\max\left(0, \frac{Q(\delta_3 - \delta_4)}{2C_4}\right), 1\right\}.$$

The optimality model is represented by

$$\frac{dS}{dt} = \varphi - (1 - h_1^*(t))\frac{\gamma SI}{1 + \mu I^2} - h_2^*(t)S - d_1 S$$

$$\frac{dI}{dt} = (1 - h_1^*(t))\frac{\gamma SI}{1 + \mu I^2} - \eta I - m_1 I - d_1 I$$

$$\frac{dQ}{dt} = \eta I - h_3^*(t)Q - d_2 Q$$

$$\frac{dR}{dt} = m_1 I + h_3^*(t)Q - d_1 R$$

$$\frac{d\delta_1}{dt} = (d_1 + h_2^*(t))\delta_1 - \frac{(-1 + h_1^*(t))I\gamma(\delta_1 - \delta_2)}{1 + I^2\mu}$$

$$\frac{d\delta_2}{dt} = -C_1 + (d_1 + m_1 + \eta)\delta_2 - m_1\delta_4 - \delta_3\eta + \frac{(-1 + h_1^*(t))S\gamma(\delta_1 - \delta_2)(-1 + I^2\mu)}{(1 + I^2\mu)^2}$$

$$\frac{d\delta_3}{dt} = (d_2 + h_3^*(t))\delta_3 - h_3^*(t)\delta_4$$

$$\frac{d\delta_4}{dt} = d_1\delta_4$$

with the initial condition $S(0) = S_0, I(0) = I_0, Q(0) = Q_0, \text{and}\ R(0) = R_0$.

8. Numerical simulations

To validate our analytical conclusions, we utilized MATLAB to conduct the necessary computations. The initial conditions were set within the invariant region. The parameters were assumed as in Table 6 with $\gamma = 1.9 \times 10^{-10}$, so that $\Re_0 = 0.9778 < 1$.

The selected parameter set corresponds to a controlled epidemic scenario, in which the basic reproduction number remains slightly below unity, representing a situation where disease transmission gradually declines because of implemented preventive measures and recovery mechanisms.

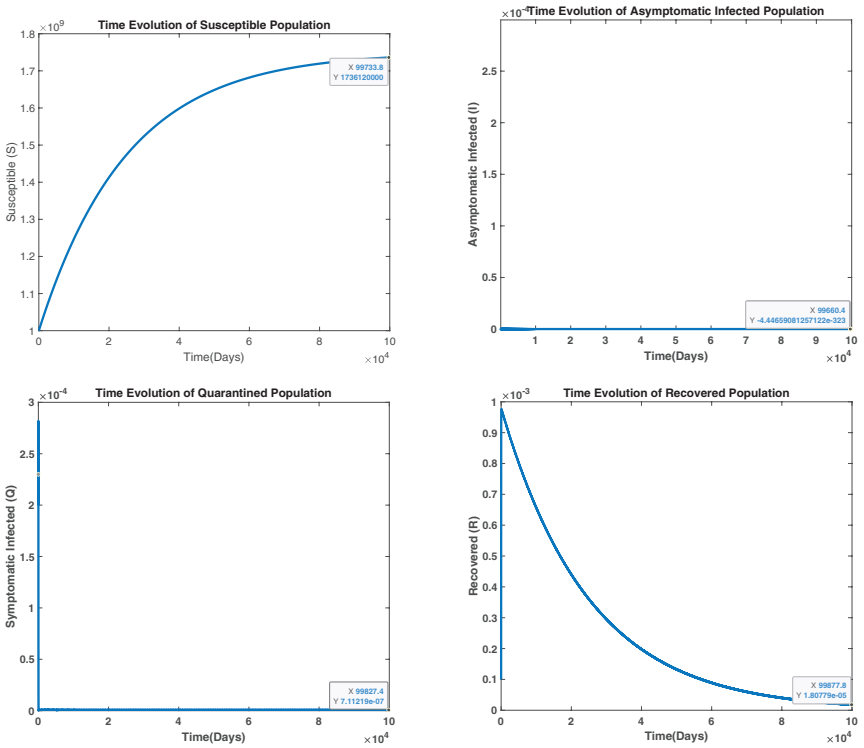

Figure 4: Time series of populations for $\Re_0 < 1$

When $\Re_0 = 0.9778$, disease propagation slows and eventually stops, leading to an increase in susceptible individuals as the illness dies out. Asymptomatic individuals start at 3×10^{-4}, reach and remain zero throughout evolution. Symptomatic individuals are initially 2.8×10^{-4} and immediately reach and then remain zero throughout the evolution because the average incidence of new cases

Table 6: Parameters and their values

Parameters	φ	γ	η	μ	m_1	m_2	d_1	d_2
Values	70000	3×10^{-10}	0.2	2×10^{-16}	0.14	0.1	4×10^{-5}	10^{-4}

is low. The recovered population first grows to 1×10^{-3} as people recover from illness. However, as new infections decrease, the number of recovered people gradually drops to zero over time. As shown in Fig. 4, the system approaches the DFE point $N^0(1.75 \times 10^9, 0, 0, 0)$ as $t \to \infty$, validating the LAS and GAS of the DFE point N^0 as stated in Theorems 3 and 6.

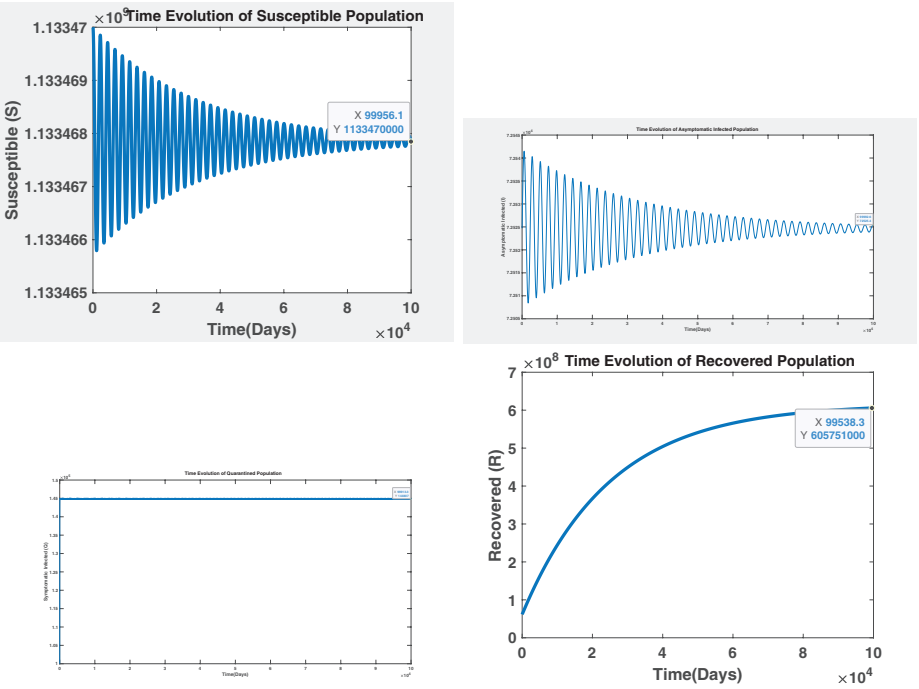

Figure 5: Time series of populations for $\Re_0 > 1$

The values of the input variables are expected to match those in Table 6, which result in $\Re_0 = 1.5439 > 1$. Susceptible individuals show early spikes from 1.133466×10^9 to 1.13347×10^9, and the fluctuation gradually decreases until it approaches the EE point, when the rate of transmission increases and the

rate of inhibition declines. Asymptomatic individuals show an early rise from 7.251×10^4 to 7.254×10^4 and the fluctuation gradually lowers until it approaches N^*. The number of symptomatic people initially climbs from 1×10^5 to 1.44×10^5 and subsequently remains at 144 886 over the time period due to the high average quantity of new infections. The number of recovered people continuously rises from 80 000 000 to 605 807 000, with both asymptomatic and symptomatic patients recovering. As shown in Fig. 5, the system approaches the EE point $N^*(1.13347 \times 10^9,\ 72524.7,\ 144904,\ 6.16097 \times 10^8)$ as $t \to \infty$. Additionally, the conditions specified in Theorem 4, namely, $b_1 = 7.39841 \times 10^{-6} > 0$ and $b_2 = 0.0000624728 > 0$, were satisfied, ensuring the LAS of the EE point. This analysis numerically validates the analytical results, concerning the stability of the DFE and EE points.

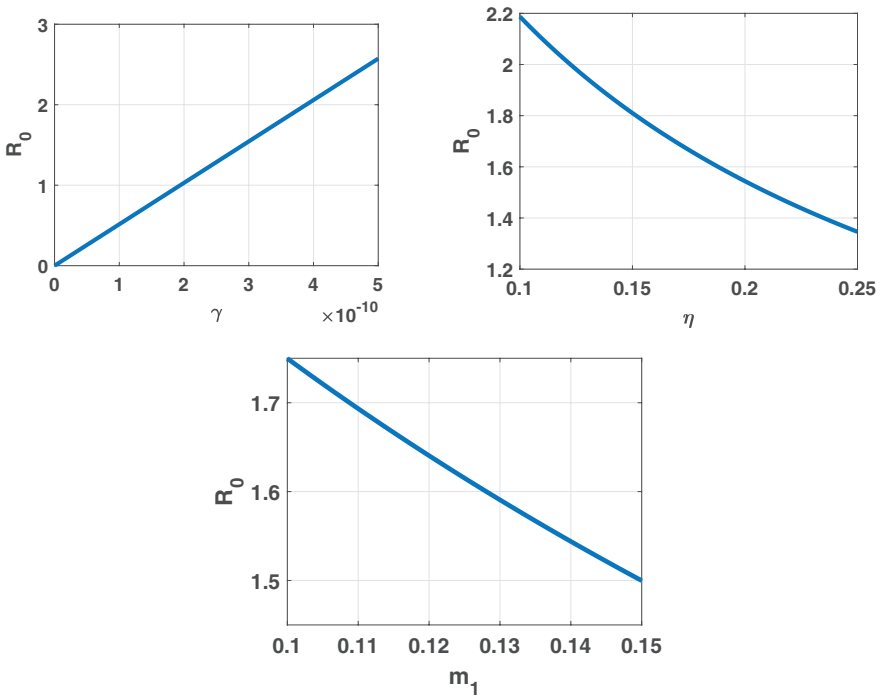

Figure 6: Behavior of BRN $\Re_0$ on the basis of γ, η, and m_1

Figure 6(a) shows that an increase from 0 to 5×10^{-10} in the transmission rate of infection (γ) regarding persons becoming infected without symptoms increases BRN by 2.5. This means that each sick person transfers the infection to at least one other person, causing the disease to become endemic. This

transition signifies a shift towards the EE, where the disease affects all people steadily. Figure 6(b) shows that increasing the rate of infection (η) from people who exhibit no symptoms to those who experience symptoms leads to a relative decrease in the basic reproduction number, BRN, from 2.2 in the BRN to 1.2. When the BRN is less than one, it indicates that the disease cannot sustain its spread within the population, implying progress toward disease eradication. Figure 6(c) shows that increasing the recovery rate (m_1) from 0.1 to 0.15 results in a decrease in the BRN value to 1.5. This drop means that, on average, each sick person transmits the virus to a maximum of one person, thereby decreasing the transmission of infection.

Figure 7(a) illustrates the changes in the transmission rate (γ) and asymptomatic development rate (η), offering insights into disease dynamics, depending upon the behavior of $\Re_0$ slide. Figure 7(b) presents the variations in the transmission rate and the rate of asymptomatic individuals moving to recovery (m_1) within a constant $\Re_0$ slide, providing valuable insights for optimizing intervention strategies. Figure 7(c) illustrates the changes in the asymptomatic development rate (η) and the rate of asymptomatic individuals moving to recovery (m_1) within a constant $\Re_0$ slide, offering insights into targeted interventions to control disease spread. These contour plots enhance the understanding of how adjustments in key parameters impact disease transmission and control measures, aiding in the development of effective public health strategies.

Figure 8(a) shows that the number of asymptomatic persons increases to 1.7×10^7 and 2.2×10^7, in turn, when psychological effects 3×10^{-16} and 1×10^{-16}, respectively, and then declines with time. Figure 8(b) demonstrate that the rate of the psychological effect $1x10^{-16}$ provides for a progressive increase of $4x10^7$ in the overall number of people in quarantine and treatment. The number of symptomatic persons increases to 3.1×10^7 and 3.4×10^7 when the inhibitory effect is 3×10^{-16} and 2×10^{-16}, respectively. These trends suggest that higher levels of psychological vigilance or adherence to preventive measures lead to a reduction in both asymptomatic and symptomatic infected cases, ultimately contributing to the prevention of virus spread.

From Figs. 9(a) and (b), it can be deduced that as γ increases at the rates of 30×10^{-11}, 32×10^{-11}, 34×10^{-11}, we observe the concurrent rise in numbers of both the infected people who are showing symptoms and not showing symptoms. As time passes, the numbers of reported cases start decreasing, in spite of the increase in the transmission rates. Epidemiologically, higher values of γ can indicate factors such as increased viral infection, decreased effectiveness of preventive measures, or higher contact rates among individuals, all of which contribute to the faster spread of disease.

From Fig. 10(a), we can infer that as η increases at the rates of 0.16, 0.2, and 0.24, respectively, indicating faster progression from asymptomatic to symp-

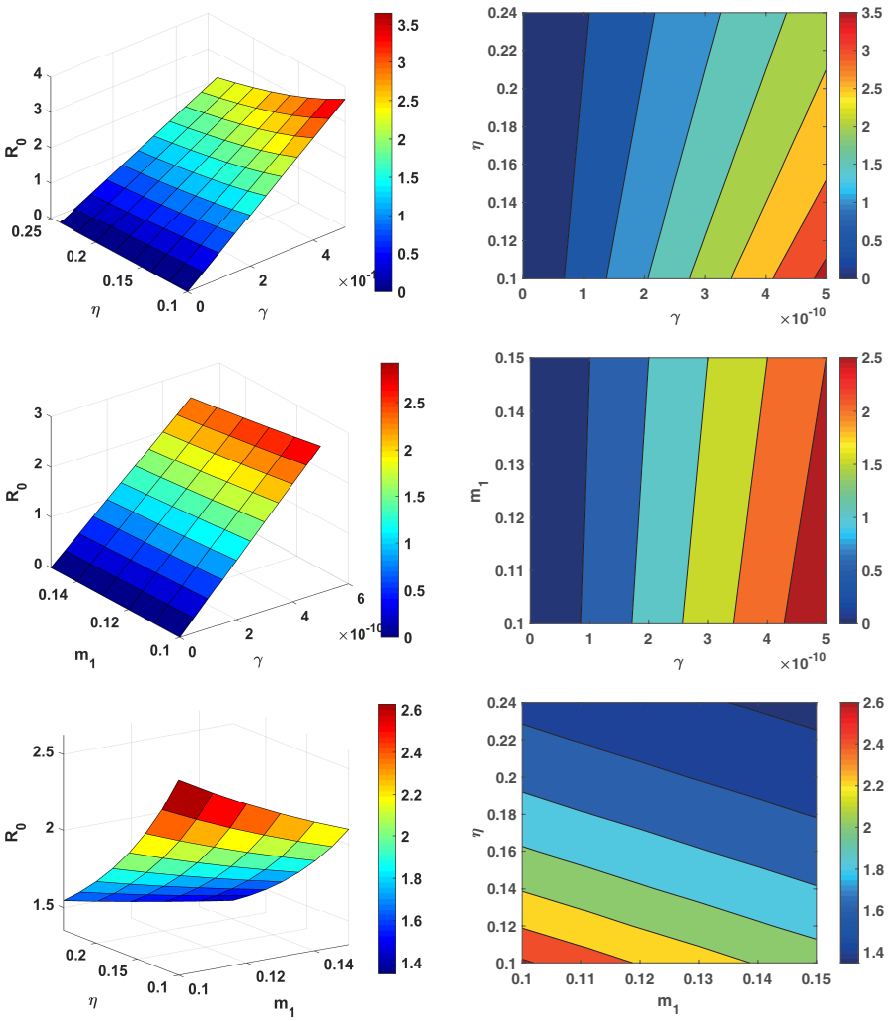

Figure 7: Contour plots illustrating the variations in γ, η, and m_1 on constant $\Re_0$ slides

tomatic infection, there is a corresponding increase of 0.6×10^7, 1.7×10^7 and 3.1×10^7, respectively, in the number of individuals infected with no symptoms (I) and corresponding decrease in the asymptomatic persons as time progresses. Figure 10(b) shows that as η increases at the rates of 0.16, 0.2, and 0.24, respectively, indicating faster progression from asymptomatic to symptomatic in-

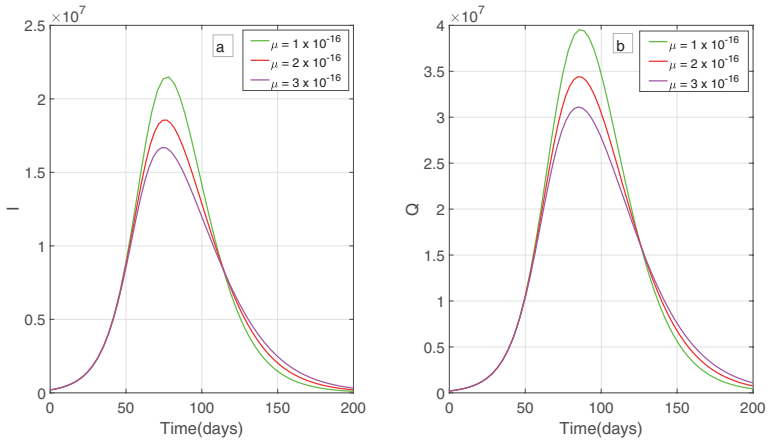

Figure 8: Time series of infected populations (a) I, (b) Q, with variations in the parameter controlling the inhibitory effect of high infection on transmission, μ

fection, there are increases of 1.5×10^7, 3.4×10^7 and 4.4×10^7, respectively, in the number of individuals infected with symptoms and in quarantine, respectively, and corresponding decreases in symptomatic individuals over time. This trend can be attributed to the fact that as more symptomatic infected individuals show symptoms of the disease and move to quarantine (Q), there is a diminishing number of asymptomatic infected individuals (I). Understanding the impact of η on disease progression is vital for assessing the dynamics of COVID-19 transmission and designing effective intervention strategies to mitigate its spread.

Figure 11(a) demonstrates that when recovery from asymptomatic infection increases at the rates of 0.1, 0.12, and 0.14, respectively, suggesting quicker recovery, the numbers of asymptomatic patients also increase. The number of people who get sick without symptoms decreases over time, from 3.1×10^7 to 1.8×10^7. Figure 11(b) demonstrates that as recovery from asymptomatic infection increases at the rates of 0.1,0.12, and 0.14, there is a concurrent increase in the numbers of infected cases with symptoms and in quarantine (Q) of 3.4×10^7, 4.4×10^7, and 5.5×10^7, respectively. The total number of people who become sick with symptoms decreases with time. This trend suggests that a greater recovery from asymptomatic infection is associated with a shorter duration of infection in both asymptomatic and symptomatic patients. Understanding the impact of m_1 on disease recovery is essential for optimizing recovery and quarantine strategies and minimizing disease transmission within the population.

After computing the optimal controls using PMP, the functions $h_i(t)$ for

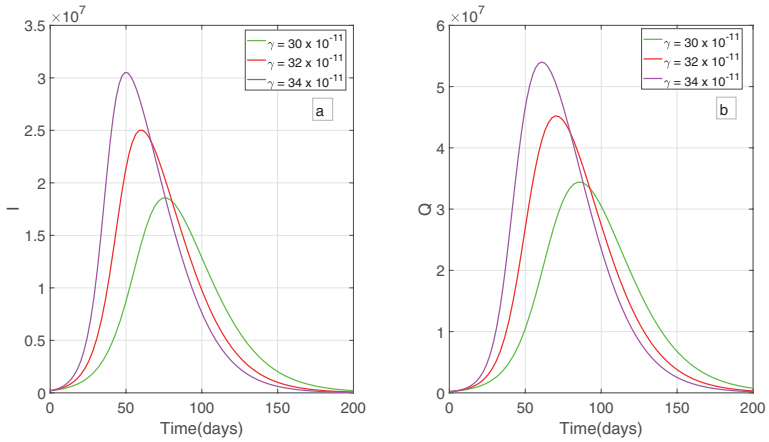

Figure 9: Time series of infected populations (a) I, (b) Q, with variation in the rate, at which susceptible people get sick without symptoms, γ

$i = 1, 2,$ and 3 are plotted individually in Figs. 12(a), (b), and (c), respectively. The control prevention measures and vaccination functions should be implemented at high intensities of 0.05 and 0.013, respectively, and then gradually reduced. This strategy helps to quickly curb the virus spread and build immunity in the population, thereby limiting the need for sustained high-intensity measures over time. In contrast, the treatment function, as shown in Fig. 12(c), indicates that the treatment rate of symptomatic individuals should start at a moderate intensity of 1×10^{-3}, increase to 6×10^{-3}, and then decrease. By implementing treatment functions, healthcare resources can be utilized optimally, and treatment capacity can be adjusted according to the fluctuating number of symptomatic cases.

The weight constants in the objective function were assumed to be $C_1 = 1 \times 10^{-7}$, $C_2 = 1 \times 10^{-7}$, $C_3 = 1 \times 10^2$, $C_4 = 1 \times 10^3$, and $C_5 = 1 \times 10^4$, and the initial values $S(0) = 14 \times 10^8$, $I(0) = 2 \times 10^5$, $Q(0) = 2 \times 10^5$, $R(0) = 15 \times 10^5$. The susceptible population of the size of 1.4×10^9 remains throughout the early stage of disease propagation, and then gradually decreases to 1.08×10^9, due to inadequate preventive and immunization measures implementation. The blue line in Fig. 13 (a) shows how the control function measures significantly reduce the susceptible population. The number of asymptomatic persons increases significantly to 1.8×10^7 when the transmission rate is 3×10^{-10}, and subsequently decreases. The blue line in Fig. 13 (b) shows that immunization and preventive measures significantly reduce the number of asymptomatic people.

The numbers of symptomatic individuals remains near zero of infection cases

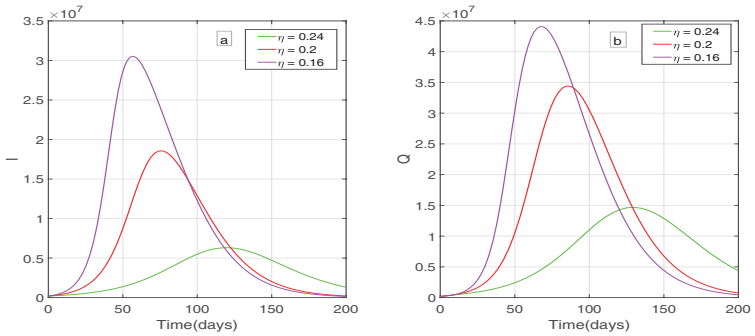

Figure 10: Time series of infected populations (a) I, (b) Q, with the variation in the rate of progression η

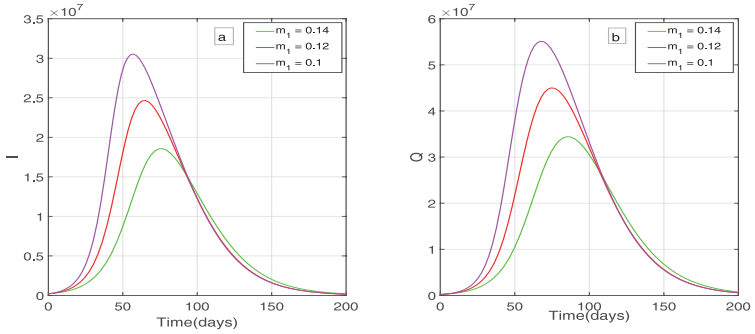

Figure 11: Time series of infected populations (a) I, (b) Q, with variation in the rate of recovery from asymptomatic infection m_1

with the help of vaccinations and prevention, which can be plotted by the blue line in Fig. 13(c). As the disease progresses, the symptomatic infected individuals recover slowly to 12.8×10^7. People are recovering as the supply of vaccinations and treatments develops, as depicted in Fig. 13(d). Compared to scenarios without the implementation of control measures, the concurrent one displays a more substantial reduction in the number of infected individuals. The success of these combined strategies underscores the importance of coordinated public health efforts in effectively managing and controlling the outbreak.

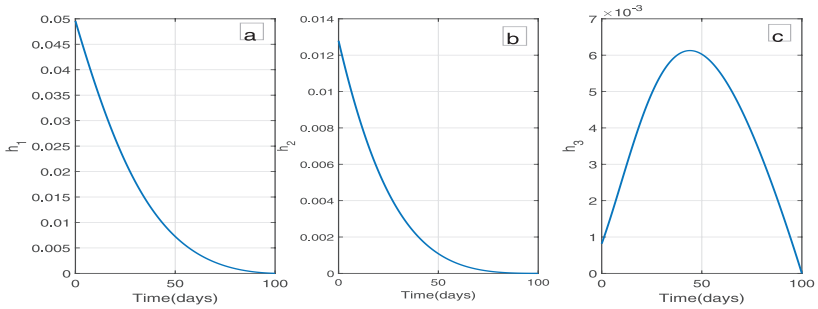

Figure 12: Trajectories of control functions (a) $h_1(t)$, (b) $h_2(t)$, and (c) $h_3(t)$.

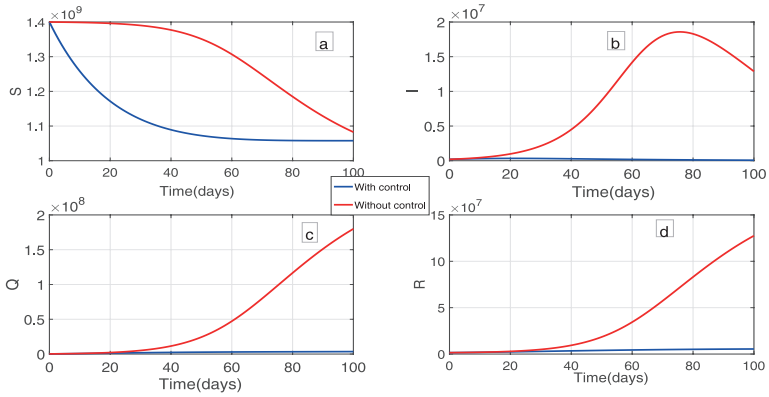

Figure 13: Time series of populations (a) S, (b) I, (c) Q, and (d) R, with implementation of all controls and without control

9. Conclusion and future scope of work

The study demonstrated the effectiveness of various control strategies in managing infection dynamics through an infection model, incorporating a non-monotonic incidence function. The BRN model was derived and utilized to determine the conditions for stability equilibria. The results indicate that when $\Re_0 = 0.9778$, i.e. less than 1, the disease propagation slows down and ultimately converges to DFE. Conversely, for the reproduction number $\Re_0 = 1.5439$, i.e. above 1, the spread of disease increases, leading to the EE. The findings provide biologically meaningful insights into how the interplay between infection rate, recovery, and control measures governs the overall epidemic trend. The study establishes a clear connection between theoretical predictions and realistic epidemic responses, emphasizing that timely and well-calibrated control policies

can significantly reduce the disease burden. Furthermore, the integration of sensitivity and optimal control analysis offers a comprehensive understanding of the system behavior under multiple intervention scenarios.

In future extensions, the model framework can also be adapted to study the combined impact of vaccination hesitancy, environmental factors, and virus mutation rates on long-term epidemic outcomes. Moreover, integrating socio-behavioral parameters and optimal resource allocation strategies will make the model more realistic and beneficial for policymakers in designing targeted intervention programs.

Appendix:

COVID-19	Coronavirus Disease 2019
BRN	Basic Reproduction Number
DFE	Disease-free Equilibrium
EE	Endemic Equilibrium
NGM	Next Generation Matrix
LAS	Locally Asymptotic stable
GAS	Globally Asymptotic stable
CCM	Castillo-Chavez method
NFSI	Normalized Forward Sensitivity Index
PMP	Pontryagin's Maximum principle
SIR	Susceptible, Infected, Recovered
SEIR	Susceptible, Exposed, Infected, Recovered

Acknowledgements

The authors would like to thank the editor and anonymous reviewers for their valuable comments and suggestions, which helped to improve the quality of the manuscript.

References

Abbasi, Z., Zamani, I., Mehra, A. H. A., Shafieirad, M. and Ibeas, A. (2020) Optimal control design of impulsive SQEIAR epidemic models with application to COVID-19. *Chaos, Solitons & Fractals*, 139, 110054.

Adalioğlu, Y. and Kaplan, Ç. (2023) A compartmental model of the COVID-19 pandemic course in Germany. *Epidemiologic Methods*, 12, 20220126.

Amaku, M., Covas, D. T., Coutinho, F. A. B., Neto, R. S. A., Struchiner, C., Wilder-Smith, A. and Massad, E. (2021) Modelling the test, trace and quarantine strategy to control the COVID-19 epidemic in the state of São Paulo, Brazil. *Infectious Disease Modelling*, 6, 46–55.

Aparecido Magrini, L., Monteiro Aguiar Baroni, M. P., Goulart, A. and Cilene Gadotti, M. (2023) Correlations between COVID-19 cases and temperature, air humidity, and social isolating rate with cross wavelet transform and wavelet coherence: Case study of New York and São Paulo cities. *Chaos: An Interdisciplinary Journal of Nonlinear Science*, 33.

Asker, E., Dhongde, S. and Shonchoy, A. S. (2025) COVID-19 and mortality among infants: Evidence from India. *Journal of Health Economics*, 101, 102991.

Bai, J. and Wang, J. (2024) Modeling long COVID dynamics: Impact of underlying health conditions. *Journal of Theoretical Biology*, 576, 111669.

Bandekar, S. R. and Ghosh, M. (2022) A co-infection model on TB-COVID-19 with optimal control and sensitivity analysis. *Mathematics and Computers in Simulation*, 200, 1–31.

Bao, S. and Hu, Z.-H. (2023) A new model of the transmission dynamics of COVID-19 propagation with vaccination and recommended treatments. *Nonlinear Dynamics*, 111, 20465– 20484.

Butt, A. I. K., Imran, M., Batool, S. and Nuwairan, M. A. (2023) Theoretical analysis of a COVID-19 CF-fractional model to optimally control the spread of pandemic. *Symmetry*, 15, 380.

Castilho, C., Gondim, J. A. M., Marchesin, M. and Sabeti, M. (2020) Assessing the efficiency of different control strategies for the COVID-19 epidemic. *Electronic Journal of Differential Equations*, 2020, 1–17.

Castillo-Chavez, C., Blower, S., van den Driessche, P., Kirschner, D. and Yakubu, A.-A., eds. (2002) *Mathematical Approaches for Emerging and Reemerging Infectious Diseases: Models, Methods, and Theory.* **IMA 126**, Springer Science & Business Media.

Chaharborj, S. S., Chaharborj, S. S., Hassan-Zadeh Asl, J. and Phang, P. S. (2021) Controlling of pandemic COVID-19 using optimal control theory. *Results in Physics*, 26.

Cheng, K. and Qiao, Y. (2025) Bifurcation and stability analysis and control strategy study of a class SEIWR infectious disease models considering viral loads in the environment. *Chaos, Solitons & Fractals*, 198, 116490.

Choi, W. and Shim, E. (2021) Optimal strategies for social distancing and testing to control COVID-19. *Journal of Theoretical Biology*, 512, 110568.

De Oliveira, K. C., Batista, T. A., Chui, D. S. and Silva, G. C. (2023) Identification of the COVID-19 epidemiological dynamics at State of Amazonas and optimal vaccination strategy proposal. *Journal of the*

Brazilian Society of Mechanical Sciences and Engineering, 45, 630.

Demongeot, J., Griette, Q., Magal, P. and Webb, G. (2022) Modeling vaccine efficacy for COVID-19 outbreak in New York city. *Biology*, 11, 345.

Dinagde, D. D., Degefa, B. D., Kitil, G. W., Feyisa, G. T. and Marami, S. N. (2024) SARS-CoV-2 infection after COVID-19 vaccinations among vaccinated individuals, prevention rate of COVID-19 vaccination: A systematic review and meta-analysis. *Heliyon*, 10.

Egeskov-Cavling, A. M., Hansen, C. L., Johannesen, C. K., Lindegaard, B., Bhatt, S., Viboud, C. and Fischer, T. K. (2025) Excess mortality and hospitalisations associated with respiratory syncytial virus, influenza, and COVID-19 among adults in Denmark (2015– 2024): a modelling study. *The Lancet Regional Health–Europe*, 55.

González-Parra, G., Cogollo, M. R. and Arenas, A. J. (2022) Mathematical modeling to study optimal allocation of vaccines against COVID-19 using an age-structured population. *Axioms*, 11, 109.

Goswami, N. K., Olaniyi, S., Abimbade, S. F. and Chuma, F. M. (2024) A mathematical model for investigating the effect of media awareness programs on the spread of COVID-19 with optimal control. *Healthcare Analytics*, 5, 100300.

Hassan, A. H., Aldila, D., Aziz, M. H. N., Kamalia, P. Z. and Peter, O. J. (2025) An Optimal Control Problem for a Monkeypox Transmission Model with Activity-Driven Contact Patterns. *Brazilian Journal of Physics*, 55, 213.

Herdicho, F. F., Fatmawati, F., Alfiniyah,C., Fajrin, F. P., Bonyah, E., Rois, M. A. and Peter, O. J. (2025) Modeling the Dynamics of Dengue Transmission with Awareness and Optimal Control Analysis. *PLoS One*, 20, e0322702.

Hu, L. and Nie, L.-F. (2021) Dynamic modeling and analysis of COVID-19 in different transmission process and control strategies. *Mathematical Methods in the Applied Sciences*, 44, 1409–1422.

Kar, T. K. and Batabyal, A. (2011) Stability analysis and optimal control of an SIR epidemic model with vaccination. *Biosystems*, 104, 127–135.

Kordt, A. H., Nymoen, R., Sali, B. and Bårdsen, G. (2025) Econometric modelling of public health and the economy: COVID-19 in Norway. *Economic Analysis and Policy*, 88, 1633–1651.

Kouidere, A., Youssoufi, L. E., Ferjouchia, H., Balatif, O. and Rachik, M. (2021) Optimal control of mathematical modeling of the spread of the COVID-19 pandemic with highlighting the negative impact of quarantine on diabetics people with cost-effectiveness. *Chaos, Solitons & Fractals*, 145, 110777.

Kumar, P., Basu, S., Santra, P. K., Ghosh, D. and Mahapatra, D. G. (2022) Optimal control design incorporating vaccination and treatment

on six compartment pandemic dynamical system. *Results in Control and Optimization*, 7, 100115.

Kumar, P., Mahapatra, D. G., Parshad, R. and Santra, P. K. (2023) Dynamical behavior and sensitivity analysis of a dengue reinfection model for vertical transmission incorporating multiple control strategies. *Communications in Mathematical Biology and Neuroscience*, 2023:134.

Lahrouz, A., Omari, L., Kiouach, D. and Belmaâti, A. (2012) Complete global stability for an SIRS epidemic model with generalized non-linear incidence and vaccination. *Applied Mathematics and Computation*, 218, 6519–6525.

Lalaoui Ben Cherif, S. M., Balatif, O. and Kebiri, O. (2024) Analysis and optimal control of a vaccinated pandemic COVID-19 model. *Journal of Mathematical Sciences*, 280, 582–604.

Ma, W., Ma, N., Dai, C., Chen, Y. and Wang, X. (2025) Fractional modeling and optimal control strategies for mutated COVID-19 pandemic. *Mathematical Methods in the Applied Sciences*, 48, 7767–7791.

Mathieu, E., Ritchie, H., Rodés-Guirao, L., Appel, C., Gavrilov, D., Giattino, C., Hasell, J., Macdonald, B., Dattani, S., Beltekian, D., Ortiz-Ospina, E. and Roser, M. (2020) COVID-19 Pandemic. *Our World in Data*, https://ourworldindata. org/coronavirus.

Nana-Kyere, S., Okyere, E. and Ankamah, J. D. G. (2020) Compartmental SEIRW COVID-19 optimal control model. *Communications in Mathematical Biology and Neuroscience*, 2020.

Oguntolu, F. A., Peter, O. J., Omede, B. I., Balogun, G. B., Ajiboye, A. O. and Panigoro, H. S. (2025) Mathematical modeling on the transmission dynamics of diphtheria with optimal control strategies. *Jambura Journal of Biomathematics (JJBM)*, 6, 1–22.

Omame, A., Isah, M. E. and Abbas, M. (2023) An optimal control model for COVID-19, zika, dengue, and chikungunya co-dynamics with reinfection. *Optimal Control Applications and Methods*, 44, 170–204.

Omorogie, E. O., Owolabi, K. M. and Olabode, B. T. (2024) A nonlinear deterministic mathematical model for investigating the population dynamics of COVID-19 in the presence of vaccination. *Healthcare Analytics*, 5, 100328.

Pantha, B., Mohammed-Awel, J. and Vaidya, N. K. (2022) Effects of vaccination on the transmission dynamics of COVID-19 in Dougherty County of Georgia, USA. *Journal of Biological Systems*, 30, 553–583.

Pei, L. and Liu, D. (2023) Long-term prediction of the COVID-19 epidemics induced by Omicron-virus in China based on a novel non-autonomous delayed SIR model. *Journal of Physics A: Mathematical and Theoretical*, 56, 235601.

Ruan, S. and Wang, W. (2003) Dynamical behavior of an epidemic model with a nonlinear incidence rate. *Journal of Differential Equations*, 188, 135–163.

Sharma, S. and Samanta, G. (2015) Stability analysis and optimal control of an epidemic model with vaccination. *International Journal of Biomathematics*, 8, 1550030.

Tchoumi, S. Y., Schwartz, E. J. and Tchuenche, J. M. (2024) A deterministic model of COVID-19 with differential infectivity and vaccination booster. *Decision Analytics Journal*, 10, 100374.

Tegegn, T. A. and Terefe, Y. A. (2025) Contribution of the 2021 COVID-19 vaccination regime to COVID-19 transmission and control in South Africa: A mathematical modeling perspective. *Chaos, Solitons & Fractals*, 199, 116870.

Teklu, S. W., Bonyah, E., Gümüş, M., El-Mesady, A., Peter, O. J. and Adel, W. (2025) Bifurcation and optimal control analysis for a fractional-order model of drug-resistant HBV infection. *Computers in Biology and Medicine*, 198, 111209.

Tian, T., Tan, J., Luo, W., Jiang, T., Chen, M., Yang, S., Wen, C., Pan, W. and Wang, X. (2021) The effects of stringent and mild interventions for coronavirus pandemic. *Journal of the American Statistical Association*, 116, 481–491.

Van den Driessche, P. and Watmough, J. (2002) Reproduction numbers and sub-threshold endemic equilibria for compartmental models of disease transmission. *Mathematical Biosciences*, 180, 29–48.

Wang, L., Zhang, X. and Liu, Z. (2018) An SEIR epidemic model with relapse and general nonlinear incidence rate with application to media impact. *Qualitative Theory of Dynamical Systems*, 17, 309–329.

World Health Organization (2024) COVID-19 Dashboard. Accessed: 2024-09-28.

Xu, C., Cheng, K., Dai, L. Guo, S. and Liu, X. (2025) Demand assessment of the number of inpatient beds in China based on the COVID-19 dynamical model. *International Journal of Biomathematics*, 18, 2350098.

Yaşar, A. and Yalçın, N. (2024) The effect of the COVID-19 pandemic on accrual-based earnings management: Evidence from four most affected European countries. *Heliyon*, 10, e29890.

Yildiz, B., Haspolat, E., Yilmaz, A. and Öneş, Z. (2022) Stability analysis and numerical simulation of dynamic and fractional SEIRD models for spread of nCOVID-19 in Turkey. *Asian-European Journal of Mathematics*, 15, 2250226.

Zamir, M., Abdeljawad, T., Nadeem, F., Khan, A. and Yousef, A. (2021) An optimal control analysis of a COVID-19 model. *Alexandria Engineering Journal*, 60, 2875–2884.

Zhang, X., Yang, L., Chen, T., Wang, Q., Yang, J., Zhang, T., Yang, J., Zhao, H., Lai, S., Feng, L. et al. (2024) Predicting influenza-like illness trends based on sentinel surveillance data in China from 2011 to 2019: A modelling and comparative study1. *Infectious Disease Modelling*, 9, 816–827.